Fizika Nizkikh Temperatur, 2011, v. 37, No. 4, p. 456–462

Infrared spectroscopy of solid normal hydrogen doped with CH_3F and O_2 at 4.2 K: CH_3F:O_2 complex and CH_3F migration

L. Abouaf-Marguin and A.-M. Vasserot

Laboratoire de Physique Moléculaire pour l'Atmosphère et l'Astrophysique, Université Pierre et Marie Curie-Paris 6, CNRS UMR7092, Paris F-75005, France
E-mail: luce.abouaf@upmc.fr

Received August 26, 2010

Double doping of solid normal hydrogen with CH_3F and O_2 at about 4.2 K gives evidence of (ortho-H_2)$_n$:CH_3F clusters and of O_2:CH_3F complex formation. A FTIR analysis of the time evolution of the spectra, in the ν_3 C–F stretching mode region, points out a behavior of the clusters very different from that of (ortho-H_2)$_n$:H_2O clusters. The main point is the observation of CH_3F molecules migration in solid para-H_2 at 4.2 K, which is a behavior different from H_2O in identical experimental conditions. This is proved by the increase with time of the CH_3F:O_2 complex integrated intensity with a rate constant $K = 2.7(2) \cdot 10^{-4}$ s^{-1}.

PACS: 33.20.Ea Infrared spectra;
36.40.–c Atomic and molecular clusters.

Keywords: matrix isolation, solid hydrogen, CH_3F:O_2 complex, nuclear spin conversion, infrared spectroscopy.

1. Introduction

If room temperature normal hydrogen ($n$$H_2$, 75% ortho-$H_2$ with total nuclear spin I = 1, and 25% para-H_2 with total nuclear spin I = 0) is condensed on a cold substrate at cryogenic temperatures (< 5 K), the ortho-H_2 concentration within the solid remains nearly constant on the order of days. Indeed, in solid hydrogen mainly hcp structured, H_2 molecules are almost free rotors and nuclear spin conversion between ortho and para states is forbidden [1,2]. Therefore, solid normal hydrogen freshly condensed is composed of 25% para-H_2 molecules ($p$$H_2$) ($J$ = 0, total spin I = 0, degeneracy 1) with no electric quadrupole moment (spherical symmetry), and 75% ortho-H_2 molecules ($o$$H_2$) ($J$ = 1, total spin I = 1, degeneracy 3) with a quadrupole moment. Furthermore, ortho molecules can migrate inside the crystal. The nuclear spin transition requires a magnetic field gradient, and in solid normal hydrogen a very slow conversion ortho to para of the H_2 molecules is observed due to interaction between neighboring $o$$H_2$ molecules. This self-conversion is assisted by the diffusion of ortho molecules, which are delocalized inside the crystal [3,4]. A doping with a paramagnetic molecule such as O_2 enhances very efficiently the conversion (catalyzed conversion).

In solid $p$$H_2$, dopant molecules such as H_2O [5,6], CH_4 [7–10] and HCl [11], trapped in high-symmetry single substitutional sites with 12 nearest neighbors, undergo almost free rotation. The CH_3F molecule rotates only about its C_3 axis [12], and always carries a nonzero total nuclear spin (I = 3/2 or 1/2).

Via their quadrupole moment, $o$$H_2$ molecules interact more strongly than $p$$H_2$ ones with dopant molecules, and are particularly able to form clusters with H_2O and CH_3F in solid H_2. For H_2O [13], a nonstatistical cluster distribution of ($o$$H_2$)$_n$:$H_2O$ clusters have been identified (n = 1 to 11) using IR spectroscopy, and their evolution with time in O_2 doped solid normal hydrogen has been simulated [14]. ($o$$H_2$)$_n$:$CH_3F$ clusters have been identified (n = 1 to 12) in $p$$H_2$ crystals where the amount of $o$$H_2$ was systematically varied from low (300 ppm) to high concentrations (> 3%) [15–17]. In $p$$H_2$ solids containing high levels of $o$$H_2$, even larger ($o$$H_2$)$_n$:$CH_3F$ clusters (n > 12) are observed, with $o$$H_2$ molecules in the second solvation shell.

The present paper is devoted to an analysis of the time evolution of the ($o$$H_2$)$_n$:$CH_3F$ clusters, hereafter labeled as CL_n, observed in the ν_3 vibrational range (C–F stretching) via IR spectroscopy, in solid normal H_2 at 4.2 K. Doping with O_2 is used to accelerate the o/p conversion process in solid $n$$H_2$. A brief description of the experimental conditions is given in Sec. 2. The spectroscopic observations are

detailed in Sec. 3, for concentrations $CH_3F/O_2/H_2$ = = 1/0/4000, 1/10/6000 and 1/20/4000, with kinetic analysis using spectral decompositions. The discussion in Sec. 4, is centered on the CH_3F:O_2 complex assignment and time evolution, and analyzes the differences between H_2O and CH_3F behaviors. In the conclusion, Sec. 5, we point out some questions raised by the present results.

2. Experimental procedures

The experimental setup has already been used extensively for rare gas matrices [18,19]. Briefly, hydrogen (purity N55, supplied by Alphagaz), H_2O (doubly distilled and degassed), O_2, CH_3F and CH_4 are premixed at various concentrations to ensure the homogeneity of the gaseous mixture, and premixing favors complex formation [20]. A solid polycrystalline film is obtained by deposition of the gas mixture onto a cold gold-coated mirror, at a rate of about 9 mmol/h, with deposition times ranging from 30 to 60 min, depending on dopant concentration and desired absorbance. The temperature of 4.2 K, is given by a calibrated silicon diode sensor embedded in the OFHC copper block of the mirror, and monitored by a S.E.R.2i BHT2400 temperature regulator, to get rid of slow drifts or oscillations, which are finally below ±0.02 deg [21]. The samples thickness is approximately 40 to 60 μm, and its homogeneity is controlled by scanning a 2 scans spectrum every 5 torr deposited. The temperature gradient due to the spectrometer light is weaker than 1 deg. Indeed, the nuclear spin conversion time of H_2O diluted in solid Ar (1/2000) is identical when irradiated permanently by the globar light and irradiated only 15% of the time [21,22]. Infrared spectra are recorded with a Bruker IFS113v FTIR spectrometer, with ~ 0.15 cm^{-1} and ~ 0.2 cm^{-1} resolution at 2000 and 4000 cm^{-1}, respectively. The time dependence of absorptions is obtained by calculating integrated intensities of the relevant IR features in each spectrum recorded with 40 scans.

3. Spectroscopic analysis

3.1. General observations

The oH_2 concentration as a function of time is studied using solid hydrogen IR absorption features recorded between 4000 and 5000 cm^{-1} and the empirical law of Ref. 23. The time dependence of the oH_2 concentration for a CH_3F/H_2 = 1/4000 doped nH_2 solid has been reported previously [24]. A fit of the data to a first-order rate law gives a time constant of 2520 min, which is slightly less than the self-conversion time constant of 3570 min indicating CH_3F can catalyze *o*/*p* conversion within the nH_2 solid. For the samples co-doped with O_2, $CH_3F/O_2/H_2$ = = 1/10/6000 and 1/20/4000, the data again fit well to a first-order rate law with time constants of about 1960 and 680 min, respectively [24]. Under these conditions the oH_2 decay is predominantly catalyzed by O_2 since it is present at much higher concentrations than CH_3F.

At time $t = 0$, for an oH_2 concentration above 60% [23], the CH_3F spectrum exhibits several structures between 600 and 4000 cm^{-1} related to the different vibrations of $^{12}CH_3F$, mainly ν_3 (~1033 cm^{-1}), ν_6 (~1183 cm^{-1}), ν_2 (~1460 cm^{-1}), ν_5 (~1470 cm^{-1}), $2\nu_5$ (~2861 cm^{-1}), ν_1 (~2965 cm^{-1}), and ν_4 (~3014 cm^{-1}). The most intense vibrations of isotopic $^{13}CH_3F$ also appear. A time dependence is measured for all the CH_3F absorptions, but the most dramatic and useful spectroscopic changes are observed in the region of the ν_3 ^{12}C–F stretching vibration. Indeed, in previous works [15,16], multiple resolved features appear between 1030 and 1040 cm^{-1} for the ν_3 stretching vibration, which have been assigned to $(oH_2)_n$:CH_3F clusters that form even in solid hydrogen matrices enriched in the para nuclear spin state.

3.2. Spectra at time t = 0

In freshly deposited samples, whatever the O_2 concentration, all the CH_3F molecules are embedded in large CL_n ($n > 12$) clusters. The ν_3 C–F stretching mode (Fig. 1) exhibits a single asymmetric peak which can be assigned to $(oH_2)_n$:CH_3F clusters, with $n > 12$, at a frequency (~1033 cm^{-1}) lower than that of CL_{12} (1034.5 cm^{-1}), in agreement with previous works [15,16]. The ν_3 peak observed at 1032.9 cm^{-1} without O_2 is asymmetric with a sharp edge on the low-energy side and tails toward the high-energy side. For increasing O_2 concentrations of 1/600 and 1/200, respectively, the ν_3 feature becomes broader, more and more asymmetrical, and shifts to the blue at 1033.1 and 1033.2 cm^{-1}. These spectroscopic observations are consistent with small amounts of *o*/*p* con-

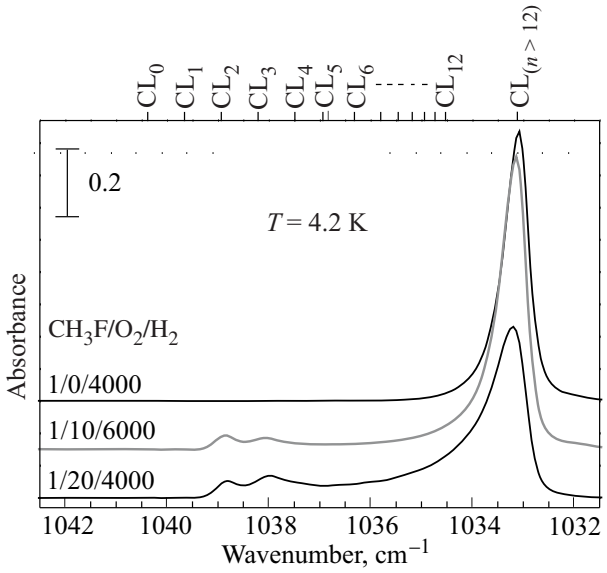

Fig. 1. Absorption spectra of CH_3F in the ν_3 mode region at time $t = 0$ for different O_2 concentrations. The frequencies of $(oH_2)_n$:CH_3F clusters [15,16] are indicated at the top of the figure.

version occurring during deposition in the samples containing O_2. In addition, two relatively broad peaks appear at 1038 and 1038.8 cm^{-1}, and the intensity of these features is obviously correlated with the O_2 concentration.

3.3. Time effects

The time dependence of the ν_3 spectra is illustrated in Fig. 2. For both samples containing O_2, the absorption assigned to clusters with $n > 12$ near 1033 cm^{-1} decreases in intensity and becomes broader while shifting to higher frequencies. These spectroscopic observations are consistent with gradual conversion of the larger CL_n clusters to smaller cluster sizes as oH_2 is converted irreversibly to pH_2. The 1038.8 cm^{-1} absorption present at time $t = 0$ increases and narrows with time, while shifting also to higher frequencies. This last feature is assigned to the CL_1 cluster that seems to be present even at early times for samples doped with O_2. It appears that clusters CL_0 and CL_1 grow directly from the decrease of clusters with $n > 6$. Clusters with n between 3 and 6 can be clearly identified for the $CH_3F/O_2/H_2$ = 1/10/6000 concentration sample (Fig. 2,*a*). A broad and weak feature labeled B, also observed in Fig. 2 of Ref. 12, grows temporarily but then stops. A small peak labeled S is observed, which has never been mentioned previously, and grows in with time at about 1038.2 cm^{-1}. This feature does not seem to belong to the CL_n cluster absorptions, and its integrated intensity is related to the O_2 concentration. It continues to grow up to the last spectrum recorded in Fig. 2,*b*.

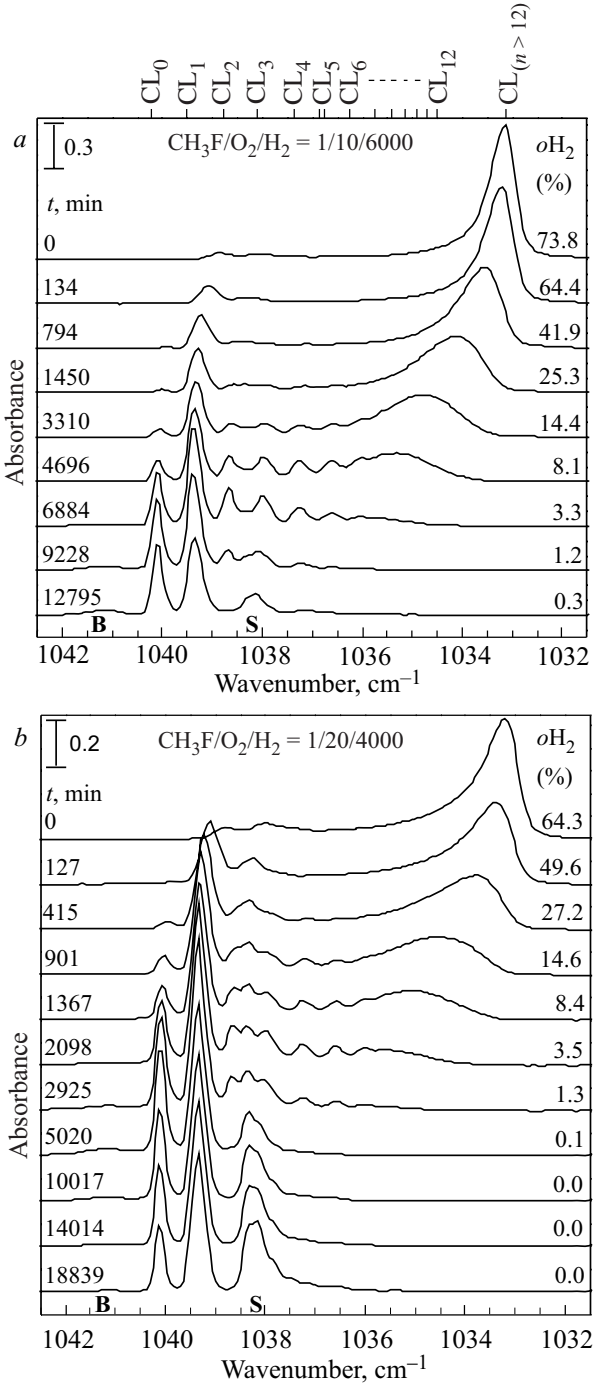

Fig. 2. Time evolution of the spectra at $T = 4.2$ K: $CH_3F/O_2/H_2$ = = 1/10/6000 (*a*); $CH_3F/O_2/H_2$ = 1/20/4000 (*b*). For B and S definitions, see text Sec. 3.3.

3.4. Spectral decompositions and kinetics

Kinetics studies based on integrated intensities calculated with fixed integration limits are not relevant here. Indeed, the CL_n cluster features are broadened by the presence of O_2 and by the high oH_2 concentrations present at early times, and thus the individual cluster features are not resolved but rather are strongly overlapping. Furthermore, each CL_n (n = 1–12) cluster peak frequency shifts with time to higher values by at least 0.5 cm^{-1}. Therefore, kinetics are based on spectral decompositions (Fig. 3) carried out with similar continuity rules as for H_2O [14], but without details for $n > 6$. The kinetic results based on these spectral decompositions are presented in Fig. 4 (integrated intensities in cm^{-1}) for the structures which

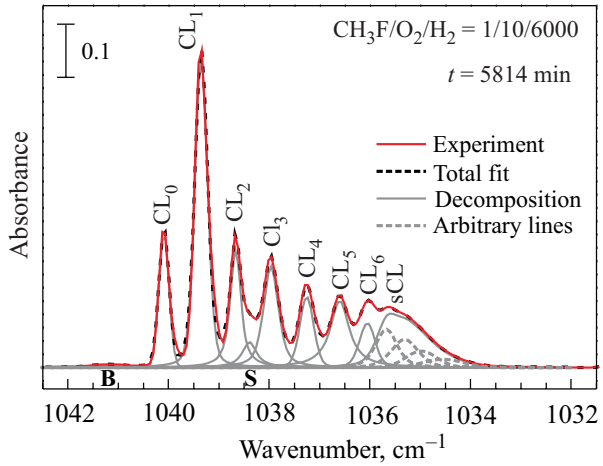

Fig. 3. Example of spectral decomposition: $CH_3F/O_2/H_2$ = = 1/10/6000. Structure S appears between CL_2 and CL_3. For sCL (clusters with $n > 6$), the decomposition (grey dotted lines) is just used to reproduce the absorption profile.

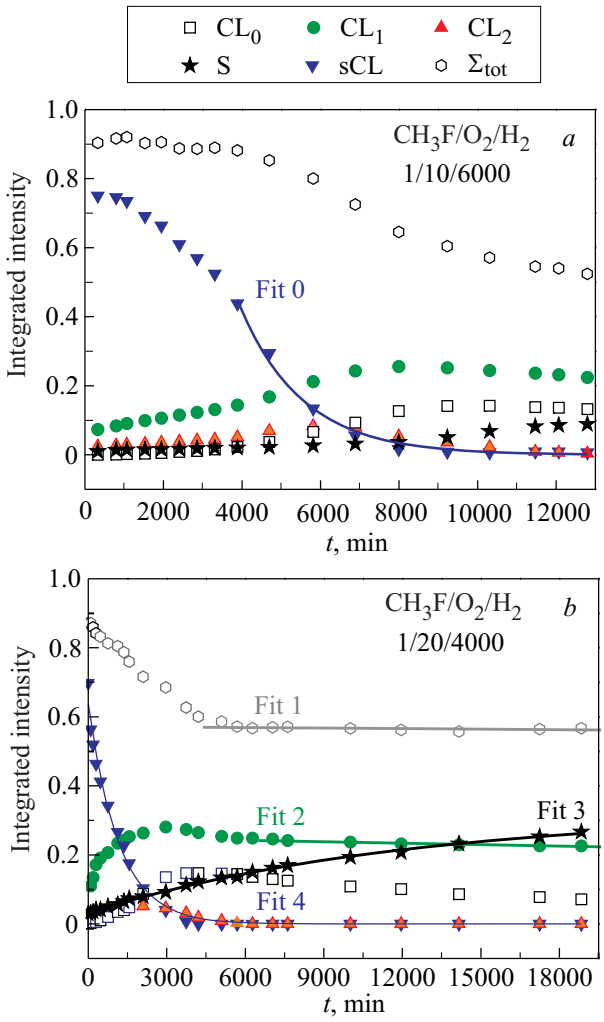

Fig. 4. (Color online) Time dependence of the integrated intensity of some structures (unit: cm^{-1}). *a* — $CH_3F/O_2/H_2$ = 1/10/6000, Fit 0: exponential decay of sCL after 4000 min, time constant τ = = 1600(90) min; *b* — $CH_3F/O_2/H_2$ = 1/20/4000, Fit 1: linear regression of Σ_{tot}, slope $5(3)\cdot10^{-7}$ min^{-1}; Fit 2: linear regression of CL_1, slope $1.8(2)\cdot10^{-6}$ min^{-1}; Fit 3: exponential growth of S, integrated intensity $I(CL_{O_2})$ fitted by the law: $I(CL_{O_2}) = \Delta I[1-\exp(t/\tau)]+I_0$, with I_0 = 0.03(1), ΔI = 0.29(1), τ = = 12200(600) min; Fit 4: exponential decay of sCL, time constant τ = 1170(55) min.

can be clearly identified: CL_0, CL_1, CL_2, S, sCL (clusters with $n > 6$), and the total integrated intensity Σ_{tot} (from 1031.5 to 1045 cm^{-1}). Intensities are corrected by the factor $[1 + 5.5\cdot10^{-6}\ t]$ (t unit: min) to account for sublimation of the sample. This sublimation correction is determined using the slow decrease of the 4505 cm^{-1} structure of H_2 observed in the $CH_3F/O_2/H_2$ = 1/20/4000 experiment after 6000 min (oH_2 concentration < 0.1%). It is weaker than the correction determined for H_2O experiments ($8.7\cdot10^{-6}$) which corresponds to sample about 4 times thicker [23]. Figures 4,*a* ($CH_3F/O_2/H_2$ = = 1/10/6000) and 4,*b* ($CH_3F/O_2/H_2$ = 1/20/4000) show similar behaviors, with evidence of an acceleration in nuclear spin conversion due to higher O_2 concentration: features at 13000 min of Fig. 4,*a* are somewhat equivalent to features at 4000 min of Fig. 4,*b* ($oH_2 \sim 0.3\%$).

The total integrated intensity Σ_{tot} of the ν_3 mode decreases during the conversion process until about 1% oH_2 concentrations (about 10000 min for 1/10/6000, and about 5000 min for 1/20/4000). At later times, only CL_0, CL_1, and structure S remain, with a constant total integrated intensity (Fig. 4,*b*, Fit 1). Therefore, the vibrational transition strength of clusters with $n > 6$ is larger than that of CL_0, CL_1 and S, and we consider that the oscillator strengths of CL_0, CL_1 and S are similar. After 6000 min, CL_1 remains almost constant (Fig. 4,*b*, Fit 2), and we can conclude that S (Fit 3) grows mainly at the expense of CL_0.

At an oH_2 concentration below 10%, in the approximation of a first-order decay, sCL vanishes with time constants of about 1600 min (Fig. 4,*a*, Fit 0) and 1170 min (Fig. 4,*b*, Fit 4) for concentrations 1/10/6000 and 1/20/4000, respectively.

4. Discussion

4.1. Assignments

The $(oH_2)_n$:CH_3F cluster assignment is straightforward from previous studies [15,16]. The broad transitory bump at 1041 cm^{-1} labeled B, seems to be an intermediate between CL_1 and CL_0. It may be CH_3F solvated in a cage of 12 pH_2 molecules (CL_0) with oH_2 molecules in the second or higher solvation shells, as observed for H_2O [14]. It disappears when the oH_2 concentration vanishes (Fig. 2,*b*).

At time t = 0, the large absorption at 1038.8 cm^{-1} is assigned to CL_1. The structure S is obviously related to the O_2 concentration. A complete analysis of the spectrum from 400 to 5000 cm^{-1} did not allow to detect any unexpected impurity, so that S can be assigned confidently to the complex CH_3F:O_2, hereafter labeled as CL_{O_2}. It originates in the asymmetric feature at ~1038 cm^{-1} (Fig. 1) most pronounced at long times.

4.2. CH_3F *diffusion: the* CH_3F:O_2 *complex*

Based on the integrated intensities of feature S and CL_0, it appears that the concentration of CH_3F:O_2 is growing at the expense of CH_3F solvated completely by pH_2 molecules. This can be explained by a migration of CH_3F molecules when not clustered to oH_2. Indeed, O_2 is not supposed to migrate under these conditions, as the H_2O:O_2 complex does not grow with time under analogous conditions. Therefore, the growth of the CH_3F:O_2 complex can be modeled by a diffusion controlled mechanism since the two molecules probably stick to each other to form irreversibly the complex as soon as they are in nearest neighbor positions, with almost no activation energy. It is not in the scope of this work to develop a detailed analysis of the diffusion, and we only draw up a balance of the process

through the law of mass action, corresponding to the elementary reaction:

$$CH_3F + O_2 \rightarrow CH_3F:O_2,$$

where the O_2 concentration ($C_{O_2} = 1/600$ or 1/200) is much higher than that of the CH_3F molecules ($C_{CH_3F} =$ = 1/4000). Under these conditions, the rate coefficient of this reaction describes the mass transport at which reactants encounter each other [25].

The free concentrations of the two partners (CH_3F and O_2) obviously decrease with time, however, since $C_{O_2} >> C_{CH_3F}$, the O_2 concentration can be approximated as constant. If K is the reaction rate, the rate equation is

$$\frac{dC_{CH_3F}}{dt} = -KC_{CH_3F}C_{O_2}$$

and

$$C_{CH_3F} = A\exp(-KC_{O_2}t) + B\,.$$

The decrease in the number of free CH_3F molecules is balanced by the increase in $CH_3F:O_2$ clusters. Therefore, the function to be fitted for the increase of structure S can be written

$$C_{CL_{O_2}} = D\left[1-\exp\left(-\frac{t}{\tau}\right)\right] + E,$$

where the parameter E corresponds to the concentration of $CH_3F:O_2$ clusters formed during deposition, before time $t = 0$; D represents the concentration of CH_3F molecules free to form $CH_3F:O_2$ clusters, and $1/\tau = KC_{O_2}$.

Therefore in absorption spectra the time dependence of the $CH_3F:O_2$ complex integrated intensity $I\left(CL_{O_2}\right)$ should be fitted by the law:

$$I\left(CL_{O_2}\right) = \Delta I\left[1-\exp\left(-\frac{t}{\tau}\right)\right] + I_0$$

with integrated intensities I_0 and ($\Delta I + I_0$) at times $t = 0$ and $t \rightarrow \infty$, respectively.

The analysis of the increase of S with time, for concentrations 1/20/4000 (Fig. 4,*b*, Fit 3), leads to the following values: $I_0 = 0.03(1)$, $\Delta I = 0.29(1)$, $\tau = 12200(600)$ min. It means that at 4.2 K the rate of $CH_3F:O_2$ cluster formation is $K = 2.7(2)\cdot10^{-4}$ s^{-1}. At the end of the experiment, all the CH_3F molecules are either isolated in pH_2 (CL_0), clustered with oH_2 (CL_1), or complexed with O_2. We can suppose that at infinite time all CH_3F molecules will be clustered with O_2 with a total integrated intensity of 0.32.

For concentrations 1/10/6000, such a kinetic analysis is not possible. Indeed, as observed in Fig. 2,*a* and in Fig. 3, the CL_{O_2} absorption feature is much weaker, and lies almost completely obscured below the CL_2 and CL_3 absorptions at least up to 7000 min. It grows very slowly

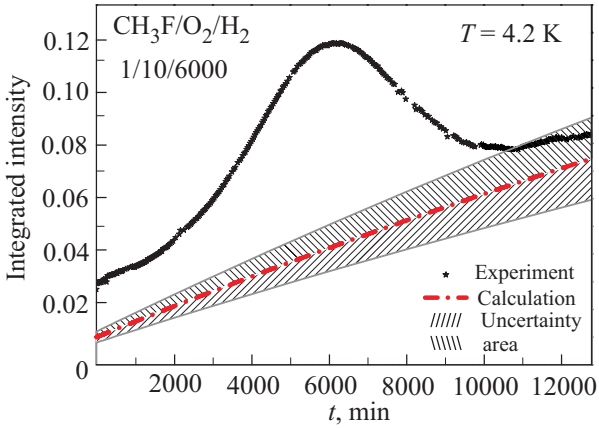

Fig. 5. (Color on line) Time dependence of the integrated intensity of structure S ($CH_3F:O_2$ complex) for concentrations $CH_3F/O_2/H_2$ = 1/10/6000. Black stars: experimental data with integration limits at 1037.54 and 1038.5 cm^{-1}, relevant behavior after 10000 min; dotted line: calculation with the law $I'\left(CL_{O_2}\right) = 0.31\,[1-\exp\,(t\,/\,54900)] + 0.01$. The uncertainty area is obtained at ± 20% of the parameters values.

(Fig. 4,*a*, black stars), as expected for this more dilute sample. Figure 5 presents the result of a careful analysis of S with integration limits adapted to the end of the experiment (1037.54 and 1038.50 cm^{-1}), when the frequencies do not shift anymore. Because the CL_{O_2} peak overlaps with CL_2 and CL_3, the integrated intensity in this range exhibits a maximum at about 6000 min. Examination of Fig. 2,*a* shows that S can only be measured reliably after ~10000 min, when the CL_2 and CL_3 absorptions vanish. Therefore, its time dependence is significant at the end of the experiment between 10000 and 13000 min, which is too short of duration for a fit.

However, both solid samples contain the same total amount of CH_3F, as confirmed by a same value of the total integrated intensity at time $t = 0$ (Fig. 4), with almost all CH_3F molecules in clusters with $n > 6$. There is then a possibility to figure out what could be the time dependence of CL_{O_2} in the more dilute sample, with a similar law:

$$I'\left(CL_{O_2}\right) = \Delta I'\left[1-\exp\left(-\frac{t}{\tau'}\right)\right] + I_0'\,.$$

Indeed $\Delta I', I_0'$ and the time constant τ', can be estimated knowing that the same CH_3F amount, in a deposition 50% times longer at similar rate, implies a thickness of the 1/10/6000 sample $e' = 1.5\,e$, if e is the thickness of the 1/20/4000 sample. Consequently:

• at time $t = 0$, some CL_{O_2} clusters are formed upon deposition with an integrated intensity $I_0 \sim 0.03$ for concentrations 1/20/4000. In the dilute sample, the CH_3F and O_2 concentrations are 1/1.5 and 1/3 times that of the concentrated sample, respectively, with $e' = 1.5\,e$. Considering in a first approach that the number of $CH_3F:O_2$ clusters formed during

deposition is roughly proportional to the concentrations and the thickness, it comes $I'_0 \sim I_0 / 3 \sim 0.01$;

• at infinite time, all the CH_3F molecules are clustered, and the total CL_{O_2} absorption should have the same value: $\Delta I' + I'_0 \sim \Delta I + I_0 \sim 0.32$. It comes: $\Delta I' \sim 0.31$;

• for 1/10/6000, as the O_2 and CH_3F concentrations are lower than for 1/20/4000, by 1/3 and 2/3 respectively, we can suppose roughly that the time constant for the cluster formation may be about 4.5 times longer: $\tau' \sim 4.5\tau \sim 54900$ min.

The kinetic equation for the dilute sample is then supposed to be roughly:

$$I'\left(CL_{O_2}\right) = 0.31\left[1 - \exp\left(-\frac{t}{54900}\right)\right] + 0.01 .$$

This approximate behavior is represented in Fig. 5 with a dotted line. All our measurements are accurate to within ± 20%. This leads us to define an uncertainty area between the 2 grey curves for the increase of the CH_3F:O_2 cluster in the dilute sample (Fig. 5). Finally, with all the overlapping problems, and knowing that integrated intensity measurements are somewhat dependent on the choice of the baseline (which is able to shift all the data), we can conclude that the increase of structure S is consistent in both experiments. It confirms the assignment of S to the CH_3F:O_2 cluster, and the diffusion of CH_3F molecules in solid p-H_2 under our experimental conditions.

4.3. Time dependence of sCL

The long observation periods presented here for these CH_3F/O_2 double doped n-H_2 samples allows the various o-H_2 to p-H_2 conversion mechanisms to be studied. During the course of the experiment there is a competition between o-H_2 self-conversion (very slow except at very high o-H_2 concentrations), O_2 catalyzed conversion which is typically more efficient than self-conversion but relies on o-H_2 migration to the O_2 catalytic center, and conversion catalyzed by CH_3F which is only active inside CL_n clusters which are at comparably low concentrations compared to O_2. For example, the shapes of the decay curves for sCL are qualitatively different for the two CH_3F/O_2 samples studied. For the 1/10/6000 sample, initially the decay in the sCL integrated intensity is very slow however it switches over to single exponential decay in the 3000–4000 min time range and then decays steadily with a time constant of 1600(90) min. Thus, for this sample the balance between o-H_2 to p-H_2 conversion processes that lead to growth and decay of $(o\text{-}H_2)_n$:CH_3F clusters with $n > 6$ turns over within this time range. In contrast, for the 1/20/4000 sample with the higher O_2 concentration, the sCL integrated intensity decays from $t = 0$ with a single exponential time constant of 1170(55) min. This suggest that for the 1/20/4000 sample the higher O_2 concentration rapidly catalyzes o-H_2 to p-H_2 conversion within the $(o\text{-}H_2)_n$:CH_3F clusters while instead for the 1/10/6000 sample, intracluster conversion by CH_3F is the dominant process.

4.4. Comparison with H_20

Experiments with CH_3F and H_2O have been performed under identical conditions, with the same amount of CO_2 atmospheric impurity at 2300 cm^{-1}. However for H_2O, clusters with $n < 12$ are only observed, and they grow and decrease in a cascade-like process [14]. The aptitude of a molecule to cluster with o-H_2 can be considered at first-order to be due to its permanent dipole moment, via a dipole-quadrupole attraction. For H_2O, the dipole moment is 1.841 D [26], and for CH_3F, it is 1.8584 D [27], only about 1% higher. It is clear that this small difference cannot explain the much stronger attraction between CH_3F and o-H_2. To go further, the London dispersion interactions, induced dipole-induced dipole interactions between instantaneous transient dipoles have to be considered. They are proportional to molecules polarizability. The polarizability of CH_3F, about 70% higher than that of H_2O [28], could be responsible for the higher ability of CH_3F to catch o-H_2 at 4.2 K. Furthermore, the ability of CH_3F to catalyze o-H_2 conversion may explain the weak growing of intermediate clusters.

Contrary to CH_3F, no H_2O migration has been observed [13,14]. At first sight, molecular migration within solid hydrogen should be related to the size and mass of the molecule. To get an order of magnitude prediction of the molecular volumes of CH_3F and H_2O, we consider the bond lengths, angles, and van der Waals radii of the atoms. For H_2O ($R_{O–H}$ = 0.9599 Å, θ_{HOH} = 104.45°) [29], we can suppose that the freely rotating molecule occupies a sphere with a diameter $D_{H_2O} \sim 3.92$ Å. The symmetric top CH_3F molecule rotating about its C_3 axis, with almost tetrahedric angles ($R_{C–H}$ = 1.0870 Å, $R_{C–F}$ = 1.3884 Å, $\theta_{HCF} \sim 110°$) [30,31], occupies a cylinder with diameter $d_{CH_3F} \sim 4.44$ Å and length $l_{CH_3F} \sim 4.31$ Å. Simple geometrical considerations do not answer the question, as CH_3F seems larger and is more massive than H_2O.

5. Conclusion

In the present work, we have shown that CH_3F is a much stronger sequester of migrating o-H_2 molecules than H_2O. It may be due to London dispersion interactions, but theoretical developments are needed.

Furthermore, differently from what we have observed for H_2O [13,14], a migration of CH_3F occurs in solid p-H_2 at about 4.2 K. It has been proved in our experimental conditions, through the increase with time of the O_2:CH_3F complex. In previous works, the very low concentrations, the short duration of the experiments, and also the low temperature, did not allow the detection of CH_3F migration. A complete study of the comparative migration of CH_3F and H_2O in solid p-H_2 would be welcome in an attempt to identify which physical (or chemical) properties of the molecules could be involved in such a process. In-

deed the potential for small molecules to migrate in solid pH_2 could be a very useful property for controlled chemical reactions.

Aknowledgment

The authors are grateful to Professor David T. Anderson for helpful discussions and constructive comments.

1. I.F. Silvera, *Rev. Mod. Phys*. **52**, 393 (1980), and references therein.
2. T. Oka, *Ann. Rev. Phys. Chem*. **44**, 299 (1993).
3. V. Shevtsov, A. Scherbakov, P. Malmi, E. Ylinen, and M. Punkkinen, *J. Low Temp. Phys*. **104**, 211 (1996).
4. V. Shevtsov, P. Malmi, E. Ylinen, and M. Punkkinen, *Physica* **B284**–**288**, 385 (2000).
5. M.E. Fajardo, S. Tam, and M.E. DeRose, *J. Mol. Struct*. **695**–**696**, 111 (2004).
6. M.E. Fajardo and C.M. Lindsay, *J. Chem. Phys*. **128**, 014505 (2008).
7. T. Momose, M. Miki, T. Wakabayashi, T. Shida, M.-C. Chan, S.S. Lee, and T. Oka, *J. Chem. Phys*. **107**, 7707 (1997).
8. S. Tam, M.E. Fajardo, H. Katsuki, H. Hoshina, T. Wakabayashi, and T. Momose, *J. Chem. Phys*. **111**, 4191 (1999).
9. M. Miki and T. Momose, *Fiz. Nizk. Temp*. **26**, 899 (2000) [*Low Temp. Phys*. **26**, 661 (2000)].
10. Y. Miyamoto, M. Fushitani, D. Ando, and T. Momose, *J. Chem. Phys*. **128**, 114502 (2008).
11. D.T. Anderson, R.J. Hinde, S. Tam, and M.E. Fajardo, *J. Chem. Phys*. **116**, 594 (2002).
12. Y.-P. Lee, Y.-J. Wu, and J.T. Hougen, *J. Chem. Phys*. **129**, 104502 (2008).
13. L. Abouaf-Marguin, A.-M. Vasserot, C. Pardanaud, J. Stienlet, and X. Michaut, *Chem. Phys. Lett*. **454**, 61 (2008).
14. L. Abouaf-Marguin, A.-M.Vasserot, and C. Pardanaud, *J. Chem. Phys*. **130**, 054503 (2009).
15. K. Yoshioka and D.T. Anderson, *J. Chem. Phys*. **119**, 4731 (2003).
16. K. Yoshioka and D.T. Anderson, *J. Mol. Struct*. **786**, 123 (2006).
17. K. Yoshioka, P.L. Raston, and D.T. Anderson, *Int. Rev. Phys. Chem*. **25**, 469 (2006).
18. X. Michaut, A.-M. Vasserot, and L. Abouaf-Marguin, *Vibrat. Spectr*. **34**, 83 (2004).
19. C. Pardanaud, A.-M. Vasserot, X. Michaut, and L. Abouaf-Marguin, *J. Mol. Struct*. **873**, 181 (2008).
20. V. Raducu, D. Jasmin, R. Dahoo, P. Brosset, B. Gauthier-Roy, and L. Abouaf-Marguin, *J. Chem. Phys*. **102**, 9235 (1995).
21. C. Pardanaud, *thesis*, Université Pierre et Marie Curie-Paris 6, pp. **75**, 160 (2007).
22. L. Abouaf-Marguin, A.-M. Vasserot, C. Pardanaud, and X. Michaut, *Chem. Phys. Lett*. **447**, 232 (2007).
23. L. Abouaf-Marguin and A.-M. Vasserot, *Chem. Phys. Lett*. **460**, 82 (2008).
24. L. Abouaf-Marguin, A.-M.Vasserot, and A. Lekic, *Chem. Phys. Lett*. **470**, 228 (2009).
25. D.F. Calef and J.M. Deutch, *Ann. Rev. Phys. Chem*. **34**, 493 (1983).
26. M.T. do N.Varella, M.H.F. Bettega, M.A.P. Lima, and L.G. Ferreira, *J. Chem. Phys*. **111**, 6396 (1999).
27. M.D. Marshall and J.S. Muenter, *J. Mol. Spectr*. **83**, 279 (1980).
28. T.N. Olney, N.M. Cann, G. Cooper, and C.E. Brion, *Chem. Phys*. **223**, 59 (1997).
29. A.F.A. Vilela, P.R.P. Barreto, R. Gargano, and C.R.M. Cunha, *Chem. Phys. Lett*. **427**, 29 (2006).
30. A. Karpfen and E.S. Kryachko, *Chem. Phys*. **310**, 77 (2005).
31. O.R. Gilliam, H.D. Edwards, and W. Gordy, *Phys. Rev*. **75**, 1014 (1949).